lubricants

MDPI

Article

Tribological and Rheological Characterization of 3D Printed Polycarbonate: Effect of Layer Orientation, Surface Topography, and Lubrication Conditions

Jovana Marković [1], Marija Matejić [1], Damjan Rangelov [2], Milan Banić [2], Jasmina Skerlić [1], Nevena Jeremić [3,4] and Miloš Matejić [5,*]

[1] Faculty of Technical Sciences, University of Priština with Temporary Settled in Kosovska Mitrovica, Knjaza Milosa 7, 38220 Kosovska Mitrovica, Kosovo; jovana.d.zivic@pr.ac.rs (J.M.)
[2] Faculty of Mechanical Engineering, University of Niš, Aleksandra Medvedeva 14, 18000 Niš, Serbia
[3] Faculty of Medical Sciences, University of Kragujevac, Svetozara Markovica 69, 34000 Kragujevac, Serbia
[4] Federal State Autonomous Educational Institution of Higher Education, I.M. Sechenov First Moscow State Medical University of the Ministry of Health of the Russian Federation, 119991 Moscow, Russia
[5] Faculty of Engineering, University of Kragujevac, Sestre Janjić 6, 34000 Kragujevac, Serbia
* Correspondence: mmatejic@kg.ac.rs; Tel.: +381-646705567

Abstract

Understanding the tribological behavior of additively manufactured polymers is essential for their reliable use in sliding components. Tribological tests were performed on a linear reciprocating tribometer pin-on-plate configuration using a polycarbonate sample (PC–PC). To assess the influence of additive-manufacturing-induced anisotropy, three build orientations (0°, 45°, 90°) were examined. Two normal loads of 39.24 N and 58.86 N, and two sliding velocities of 15 and 20 mm/s were selected to represent typical low-load operating conditions of polymeric components. Tests were conducted in dry contact and with two commercial lubricants exhibiting distinct rheological characteristics. Surface topography was characterized before and after testing to evaluate orientation-dependent roughness evolution, while rheological measurements provided effective viscosities at shear rates corresponding to imposed velocities. Frictional behavior was analyzed through the Stribeck parameter, showing that all configurations operated within boundary or early mixed lubrication regimes. Longitudinal specimen layer orientation (90°) was expected to give the lowest friction. In fact, dominant lowest friction in most of the examination regimes gave the 45° build orientation, whereas the 0° orientation hindered lubricant entrainment and produced the highest boundary interaction. Differences in lubricant viscosity influenced Stribeck positioning and the magnitude of friction reduction, demonstrating strong coupling between layer orientation, roughness evolution, and lubrication performance.

Keywords: polycarbonate; additive manufacturing; layer orientation; surface roughness; boundary lubrication; Stribeck curve; rheology; reciprocating tribometer

Received: 27 November 2025
Revised: 26 December 2025
Accepted: 5 January 2026
Published: 8 January 2026

1. Introduction

Tribology plays a fundamental role in the design, efficiency, and reliability of mechanical systems involving static or dynamic contact. Frictional losses and wear remain among the largest contributors to global energy waste, and it is estimated that nearly 23% of all primary energy consumption originates from tribological interactions, while even partial implementation of optimized friction- and wear-control strategies could significantly reduce industrial energy demand and CO_2 emissions [1,2]. As engineering systems

increasingly adopt lightweight components, polymeric materials are becoming attractive alternatives to metals due to their low density, inherent damping capability, design flexibility, and ability to function in dry or minimally lubricated conditions [3–5]. Among engineering polymers, polycarbonate (PC) stands out for its combination of high impact resistance, ductility, thermal stability, and surface durability, leading to broad use in automotive, aerospace, and industrial applications [6–8].

The development of additive manufacturing (AM), and, in particular, fused-filament fabrication (FFF), has enabled the production of complex PC components with tailored geometries. However, AM also introduces layer-dependent anisotropy, interlayer bonding imperfections, and orientation-specific surface topography, all of which strongly influence mechanical and tribological performance [9–12]. Prior research has shown that yield strength, toughness, and elastic/plastic behavior of PC directly affect its frictional response and wear resistance, particularly under boundary-dominated conditions typical for low-load systems [13–15]. Recent work by Jezný et al. [16] investigated the resistance of FDM-manufactured polycarbonate samples to abrasive action, demonstrating the influence of printing parameters on wear behavior under controlled conditions. Their findings emphasize the role of process-induced surface features on material degradation, reinforcing the need for systematic evaluation of tribological performance in FFF-produced components. Composite modifications—such as incorporating MoS_2, graphite, SiC, carbon fibers, CNTs, TiO_2, or organoclays—have been shown to improve wear resistance and reduce friction, but these benefits depend on interfacial bonding and microstructural uniformity [14,17–21]. More recently, engineered surface coatings such as Diamond-Like-Carbon films have been used to enhance surface hardness and abrasion resistance of PC, again highlighting the sensitivity of this polymer to surface-level modifications [22].

Lubrication remains one of the most effective approaches for reducing friction and extending the lifetime of polymer–polymer contacts. The performance of lubricants depends on viscosity, shear stability, temperature response, and the ability to form a continuous load-bearing film, even in oscillatory or reciprocating contacts where motion reversal disrupts hydrodynamic entrainment [5,23–25]. Recent advancements in bio-based lubricants, synthetic esters, and environmentally acceptable lubricants (EALs) have introduced new formulations with favorable thermal stability, polarity, and additive activation behavior [25,26]. For grease lubrication, rheological parameters—such as viscosity at relevant shear rates, yield stress, and shear-thinning behavior—play a dominant role in film stability in boundary and early mixed lubrication regimes, which are common in low-speed sliding of polymers [27]. While lubrication of metal–polymer and metal–metal contacts has been widely studied, PC–PC grease-lubricated contacts remain insufficiently explored, particularly in relation to additive manufacturing parameters.

In the context of AM polymers, several studies have investigated the influence of printing parameters, layer orientation, raster angle, and surface roughness on friction and wear [28,29]. The general consensus is that surface anisotropy and interlayer bonding quality significantly influence friction behavior at small loads, while higher loads increase the contribution of bulk mechanical properties and plastic deformation in the contact zone. For PC specifically, prior research has mainly focused on mechanical properties, surface integrity, dimensional accuracy, or the effect of temperature on wear, whereas systematic investigations of lubricated PC–PC sliding—and especially the interaction between layer orientation, surface-topography evolution, and lubricant rheology—are still scarce [22,26,30,31].

Despite the rapid expansion of AM technologies, three key limitations persist in the current literature. First, most studies focus on dry sliding, even though many realistic PC components operate with minimal or grease lubrication, especially in reciprocating

systems. Second, the correlation between layer-dependent surface roughness evolution and frictional response remains poorly understood, particularly before and after testing. Third, tribological and rheological properties are rarely integrated into a single analytical framework, leaving unclear how grease viscosity, yield stress, and shear-thinning behavior influence the Stribeck curve for PC–PC contacts.

These gaps are especially important for applications involving low velocities (15–20 mm/s) and low normal loads (39.24–58.86 N), in which film formation is minimal, and friction is governed primarily by asperity interactions, material compliance, and lubricant rheology. Additively manufactured PC components used in guides, sliding bushings, lightweight mechanisms, consumer products, medical devices, and robotics frequently operate under these conditions. As such, a combined analysis of tribology, lubrication behavior, surface-topography evolution, and grease rheology is essential for accurate performance prediction.

To address these gaps, the present study provides a comprehensive investigation of FFF-printed polycarbonate under controlled variations in layer orientation (0°, 45°, 90°), sliding velocity (15 and 20 mm/s), applied load (39.24 and 58.86 N), and lubrication regime (dry vs. two commercial greases). By combining linear reciprocating tribometry, detailed surface-topography evaluation before and after testing, and rheological characterization of both lubricants, this work offers one of the first integrated datasets for PC–PC tribological performance in low-speed reciprocating motion. The results are mapped onto the Stribeck parameter to clarify lubrication regime transitions. The novelty of this study lies in correlating anisotropic surface evolution with frictional behavior, evaluating how grease rheology influences boundary lubrication in polymer–polymer contacts, and providing insights relevant for the design of AM PC components in practical low-load tribosystems.

2. Materials and Methods

2.1. Fabrication of Polycarbonate Specimens

All test specimens were manufactured using a Bambu Lab X1 Carbon fused-filament fabrication (FFF) system equipped with an Automatic Material System (AMS). Polycarbonate (PC) filament supplied by Bambu Lab was used as the feedstock material. Prior to printing, the filament was dried for 12 h at 60 °C to ensure moisture-free extrusion and dimensional stability. A summary of the printer process parameters (extruder temperature, bed temperature, cooling conditions, nozzle diameter, layer height, infill density, and printing speed) is provided in [32].

The material properties of the PC filament (as tensile modulus, tensile strength, elongation, Vicar softening temperature, glass-transition temperature, impact strength, and heat-deflection temperature) are summarized in Table 1.

Table 1. Polycarbonate characteristics.

Mechanical Properties		Physical Properties	
Young's modulus (X-Y)	2110 ± 40 MPa	Density	1.20 g/cm^3
Young's modulus (Z)	2450 ± 60 MPa	Melt index	32.2 ± 2.9 g/10 min
Tensile strength (X-Y)	55 ± 4 MPa	Melting temperature	228 °C
Tensile strength (Z)	34 ± 3 MPa	Glass transition temperature	145 °C
Breaking elongation rate (X-Y)	3.8 ± 0.3%	Crystallization temperature	N/A
Breaking elongation rate (Z)	2.1 ± 0.4%	Vicar Softening temperature	119 °C
Bending modulus (X-Y)	2310 ± 70 MPa	Heat deflection temperature	117 °C
Bending modulus (Z)	1620 ± 80 MPa	Heat deflection temperature	112 °C

Table 1. *Cont.*

Mechanical Properties		Physical Properties	
Bending strength (X-Y)	108 ± 4 MPa	Saturated water absorption rate 25 °C, 55% RH	0.25%
Bending strength (Z)	55 ± 2 MPa		

All specimens were allowed to condition at 23 ± 2 °C and 50 ± 5% relative humidity for at least 48 h prior to tribological testing.

2.2. Tribological Test Rig and Contact Specimens

Tribological experiments were performed using a custom-built linear reciprocating tribometer designed to evaluate PC–PC contacts under controlled low-load and low-velocity conditions. A schematic view of the test stand is shown in Figure 1.

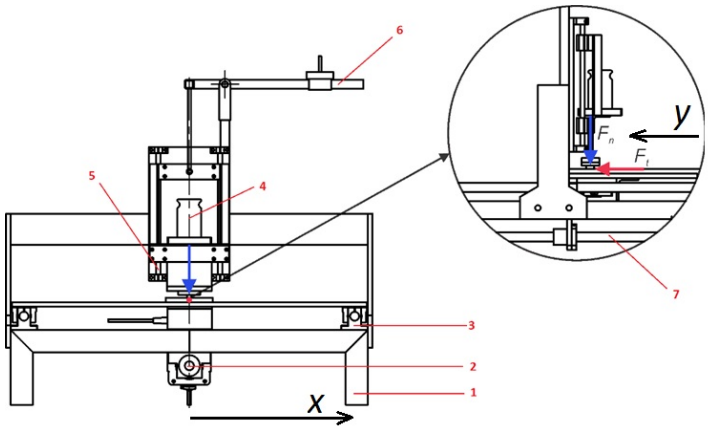

Figure 1. Schematic view of the test rig: 1—steel frame; 2—servo-step motor; 3—linear guides with bearings; 4—normal force application; 5—linear guide with bearings for normal force application; 6—counterweight; 7—linear guide with bearings for movement stabilization.

The tribometer consists of a rigid steel frame, a horizontal linear guide system, a computer-controlled servo-stepper motor, and a precision stainless-steel load carrier used to apply normal force through calibrated dead weights. The reciprocating motion is generated by a ball-screw transmission coupled directly to the motor shaft.

The normal load was applied using 4 kg and 6 kg weights, corresponding to nominal contact forces of approximately 39.24 N and 58.86 N, respectively. The sliding velocities were set to 15 mm/s and 20 mm/s, chosen to match the low-speed operating range typical for lightweight PC components. The stroke of the tribometer generated a total sliding distance of 50 m, consistent with ASTM G133 [33] and ISO 7148-2 [34] recommendations for reciprocating tribology. The stroke size was 0.35 m. The specimens were printed in three build orientations representative of typical anisotropy in FFF manufacturing—0°, 45°, and 90° relative to the printing plane, and they are shown in Figure 2.

In this study, the printing orientation is defined with respect to the build platform of the FFF process, while the sliding direction during tribological testing is fixed by the experimental setup. Accordingly, the 90° printing orientation corresponds to filament deposition paths aligned parallel to the sliding direction, whereas the 0° orientation represents filament paths oriented perpendicular to the sliding direction. The 45° orientation denotes an inclined filament arrangement relative to the sliding direction. The choice of the 0° reference orientation is directly related to the tribometer coordinate system, where the primary sliding motion is aligned with the *Y*-axis, while the perpendicular direction

corresponds to the *X*-axis, as illustrated in Figure 1. This definition is consistently applied throughout the manuscript.

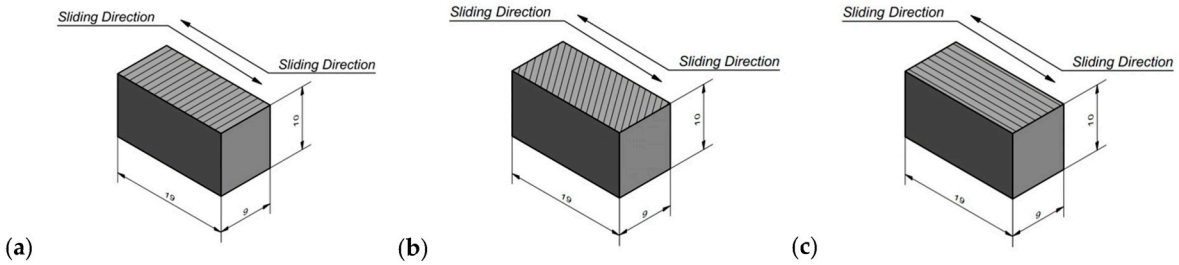

(**a**) (**b**) (**c**)

Figure 2. Schematic representation of the three printing orientations used for manufacturing the PC pin specimens: (**a**) 0° layer orientation; (**b**) 45° layer orientation; (**c**) 90° layer orientation.

The positioning and orientation of the models in the additive manufacturing process were performed in accordance with ISO 17295:2023 [35], using the 0°, 45°, and 90° build orientations (Figure 2). In addition to the test specimens, sliding tracks were printed from the same material and under identical printing conditions, also in 0°, 45°, and 90° orientations, according to longitudinal printing direction. This ensured full material and structural uniformity between the contacting surfaces (specimen–track). Each experiment was conducted using the same orientation pair (specimen and track both at 0°, both at 45°, or both at 90°). All printing parameters used in this study (e.g., nozzle and bed temperature, cooling settings, nozzle diameter, layer height, infill density, and printing speed) are reported in Table 2 to ensure reproducibility; Ref. [32] is cited only for general information on the printer platform.

Table 2. Three-dimensional printing parameters.

Parameter	Value
Layer height	0.20 mm
Line width	0.42 mm
Infill density	100%
Nozzle temperature	280 °C
Heatbed temperature	110 °C
Chamber temperature	60 °C

The dimensions of the sliding tracks were 450 × 105 mm. The dimensions of the test specimens were 18 × 9 × 12 mm, with an active contact area of 18 × 9 mm (162 mm^2). After printing, to ensure uniform starting conditions and eliminate random surface irregularities not inherent to the FFF process, all surfaces were cleaned with isopropanol.

Surface topography of the specimens was measured using a Mitutoyo surface roughness profilometer before and after testing (Figure 3). Prior to each experiment, the mass of all specimens was measured, ranging from 2.69 g to 2.72 g.

The surface topography measurements were performed using a Mitutoyo surface roughness profilometer, equipped with a high-precision stylus sensor capable of capturing fine surface irregularities. The device provides profilometric data with micrometer-level vertical resolution and is suitable for evaluating both printed and post-processed polymer surfaces. All measurements were carried out in a controlled laboratory environment, following the manufacturer's recommended scanning procedure to ensure repeatability and accuracy. All specimens' surface profiles were measured orthogonally relative to the printing orientation.

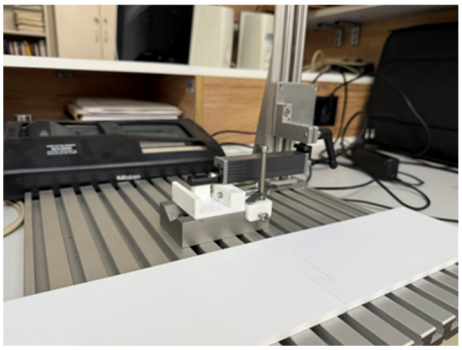

Figure 3. Mitutoyo profilometer in specimen measurement operation.

2.3. Contact Configuration and Measurement Acquisition

A pin-on-plate configuration was used, with both contacting elements fabricated from the same PC filament. The pin was fixed to a rigid holder, while the plate was mounted on the moving carriage of the tribometer. The friction force $F_\mu(t)$ was measured through a horizontal load cell, and the normal load F_n through vertical mass loading; this arrangement is illustrated in Figure 1.

The system acquired friction force and normal force simultaneously through a dedicated data acquisition unit. The coefficient of friction (COF) was calculated as in Equation (1).

$$\mu(t) = \frac{F_\mu(t)}{F_n} \quad (1)$$

The sampling frequency, filtering, and statistical post-processing are described separately in Sections 3 and 4.

Metrology and Load-Cell Calibration

A strain-gauge load cell of the S-CZL301 type (100 kg capacity) was used for friction force measurement, providing high accuracy, stability, and a linear signal response throughout the applied loading range. The key performance specifications of the sensor are summarized in Table 3.

Table 3. Technical specifications of the load-cell sensor used for normal and friction force measurement.

Parameters	Value
Rated output, mV/V	2.0 ± 0.04
Comprehensive error, %	±0.02–0.03
Zero balance, %	±1.0
Input resistance, Ω	350 ± 10
Used temperature range, °C	−20–55
Excitation voltage, V	9–12

Prior to testing, the friction load cell was calibrated using certified reference masses of 1, 2, 4, and 6 kg. The corresponding nominal forces (9.81–58.86 N) were compared with the measured load cell output to establish the calibration curve. The response of the load cell was highly linear, with a regression coefficient $R^2 > 0.999$. The maximum deviation from the nominal value was below 0.1%, confirming excellent load cell linearity and stability. The calibration results are given in Table 4.

Measurement uncertainty was determined from calibration data, sensor specifications, and the statistical dispersion observed during force acquisition. The expanded uncertainty (k = 2) of the normal force was ±0.06 N, while that of the friction force was ±0.03 N.

Table 4. Calibration results for the load cell used for normal and friction force acquisition.

Nominal Mass (kg)	Nominal Force (N)	Measured Force (N)	Deviation (%)
1 kg	9.81	9.80	–0.10%
2 kg	19.62	19.63	+0.05%
4 kg	39.24	39.22	–0.05%
6 kg	58.86	58.90	+0.07%

The coefficient of friction (COF) was computed as $\mu = Ft/Fn$, and its uncertainty was derived using standard error propagation for a quotient. Considering the uncertainties of both channels, the resulting COF uncertainty was ± 0.01 under all operating conditions.

Friction force signals were sampled at 500 Hz and processed with a second-order low-pass Butterworth filter (20 Hz cut-off), ensuring effective noise suppression while preserving the characteristics of the reciprocating motion. Prior to each test, the pin–plate assembly alignment was checked, maintaining parallelism within 50 µm to minimize parasitic force contributions.

2.4. Lubrication Conditions

Two lubricants were used for the grease-lubricated tests, hereafter denoted as Lub 1 and Lub 2. Lub 1 was an N-insulating silicone paste (AG Termopasty), which is highly versatile, suitable for maintaining rubber and plastic components in electronic devices, and for protecting them from environmental influences. It is a solid white substance that does not dissolve in water, and its high resistance to acids, bases, salts, and gases such as sulfur dioxide and ammonia ensures effective protection. The physicochemical characteristics of this lubricant are provided in Table 1. Lub 2 was a petrolatum "technica vaselina" (AG Termopasty), described as an acid-free, neutral, and chemically inert grease that protects metals, plastics, rubber, and other materials from corrosion, sticking, and drying. This grease contains no acids or additives such as MoS_2, PTFE, or graphite, and therefore does not react with polymers. It was used as a lubricating and protective medium in the PC–PC contact to reduce friction and prevent adhesive wear. The physicochemical characteristics of this lubricant are also given in Table 5.

Table 5. Physicochemical properties of lubricants.

Lub 1—*N Insulating Silicone Paste*		**Lub 2—*Techica Vaselina***	
Parameters	**Value**	**Parameters**	**Value**
Density, g/cm^3	1.02–1.04	Density, g/cm^3	~0.83
Operating temperature, °C	−40–200	Operating temperature, °C	−10–90
Penetration before processing, mm	180–220	Melting temperature, °C	54
Penetration after processing, mm	up to 270	Kinematic viscosity at 100 °C, mm^2/s	~6.87
NLGI	from 3–4 to 2.5–3		
Specific heat, kcal/kg—°C	0.3		

Rheological characterization of both lubricants was conducted at a temperature of 22 °C to determine their temperature-dependent viscosity and resistance to flow under applied shear. The rheological analysis of the lubricants was carried out using an Anton Paar MCR 102e rotational rheometer (Figure 4), with the aim of obtaining a detailed characterization of their viscoelastic and structural properties. This instrument is a high-precision system based on an advanced air-bearing drive, which ensures minimal mechanical friction and a stable response when measuring sensitive and complex materials. Experimental tests were performed using a plate–plate geometry with a serrated surface (P35/Ti/SE), with a

plate gap of 0.5 mm and a controlled temperature of 22 ± 0.1 °C, ensuring the stability and reliability of the results and eliminating potential sample slippage.

Figure 4. Anton Paar MCR 102e rotational rheometer.

Rheocompass 1.31 software was used for test parameter control, programming of loading sequences, and real-time monitoring of rheological parameter changes. The software enables detailed data analysis, including the application of appropriate rheological models to describe lubricant flow, visualization of results, and generation of graphical outputs that facilitate the interpretation of experimental findings. The integrated system for temperature, stress, and shear control ensured a high degree of precision and reliability in measurements.

2.5. Experimental Matrix

The complete test matrix is given in Table 6, which summarizes the combinations of:

- three printing orientations (0°, 45°, 90°);
- two normal loads (39.24 N and 58.86 N);
- two velocities (15 mm/s and 20 mm/s);
- two lubrication regimes (dry and two greases);
- three repetitions per condition for a total of 36 unique tests.

Table 6. Experiment matrix.

Regime	39.24 N	58.86 N	15 mm/s	20 mm/s	Orientation (0°, 45°, 90°)	No. of Replications	Total No. of Tests
Dry	1	1	1	1	3	3	12
Lub 1	1	1	1	1	3	3	12
Lub 2	1	1	1	1	3	3	12
					Total	9	36

Note: For clarity, the sample codes A1–A12 used in the surface-topography analysis correspond to the 12 unique factor combinations; their full decoding is provided in Table 7.

Table 7. Initial and after-testing parameters of 2D profiles.

Contact	Initial Roughness Pin				After Roughness Pin				Initial Roughness Plate				After Roughness Plate				Avg COF
90°	Ra	Ry	Rz	Rq	Ra	Ry	Rz	Rq	Ra	Ry	Rz	Rq	Ra	Ry	Rz	Rq	
A1	1.77	5.8	5.15	1.98	1.38	4.89	4.09	1.57	0.96	3.64	3.34	1.1	0.89	3.89	2.99	1.09	0.096
A2	2.00	4.66	4.84	2.12	1.33	4.34	4.11	1.47	0.89	3.2	2.35	1.05	0.73	3.25	2.48	0.88	0.078
A3	1.25	3.14	2.75	1.13	0.73	2.76	2.49	0.84	0.84	3.87	2.78	0.99	0.79	3.59	2.6	0.94	0.054
A4	1.29	3.55	3.11	1.65	0.83	3.16	2.8	0.96	0.96	4.32	3.69	1.19	0.79	3.49	2.91	0.96	0.066
A5	0.80	1.84	1.43	0.91	0.24	1.09	0.89	0.29	1.2	5.33	4.11	1.02	1.09	4.91	3.77	1.29	0.044
A6	1.11	2.23	2.12	0.95	0.49	1.74	1.51	0.55	1.01	4.44	3.35	1.21	0.89	3.89	2.82	1.08	0.054
A7	1.00	2.71	2.06	1.18	0.6	2.7	2.05	0.76	1.23	4.92	4.3	1.55	1.1	4.89	4.1	1.35	0.067
A8	1.08	3.11	2.91	1.17	0.53	2.65	2.48	0.64	1.46	6.43	5.21	1.8	1.15	4.98	3.69	1.38	0.075
A9	1.10	2.29	1.9	1.15	0.48	1.93	1.58	0.56	1.33	4.56	4.33	1.56	1.04	4.2	3.58	1.22	0.057
A10	0.58	2.14	1.96	0.64	0.42	2.1	1.65	0.53	1.05	4.76	3.71	1.26	0.99	4.15	3.4	1.21	0.066
A11	1.24	2.52	2.24	1.3	0.48	2.03	1.84	0.57	0.84	3.57	2.61	0.98	0.71	3.33	2.23	0.87	0.053
A12	1.00	3.1	2.74	1.09	0.59	2.49	2.11	0.69	0.98	3.9	3.22	1.02	0.84	3.5	2.72	0.98	0.065
45°	Ra	Ry	Rz	Rq	Ra	Ry	Rz	Rq	Ra	Ry	Rz	Rq	Ra	Ry	Rz	Rq	
A1	9.98	34.6	25.1	8.63	7.51	31.9	23.1	7.75	9.9	63	43.4	14.1	8.48	64.2	51.7	13	0.077
A2	6.1	40.2	29.1	7.58	6.19	32.9	21.8	6.96	8.32	51.6	36.1	11	7.35	49.6	36.2	10.9	0.072
A3	6.92	41.4	32.2	9	5.88	40.8	31.4	8.63	8.44	53	23.7	11.2	7.67	48.1	37.7	10.8	0.05
A4	6.28	36.9	22.9	8.33	10.6	36.5	22.4	7.63	12.2	61	57.9	16.1	10.4	64.6	61.6	15.1	0.062
A5	6.26	39.5	25.4	8.26	6.71	38.8	24.8	7.82	13.1	80	59.9	18.6	12	74.3	53.1	17.9	0.044
A6	6.06	39	26.3	8.35	6.89	38.2	25.8	7.57	9.83	62.5	45.6	14.3	8.63	59.9	45.4	12.4	0.06
A7	7.92	36.8	26.4	9.59	6.25	36.1	26	9.15	7.99	55.1	39.9	12.6	6.91	54.1	39.3	10.7	0.049
A8	6.20	37.3	24.6	8.08	5.69	41.2	26.9	8.24	9.01	65.3	50.8	13.5	8.37	52.6	42.5	11.7	0.065
A9	6.58	36.8	27.4	8.16	6.53	36.4	27	7.67	9.72	56.6	53.2	14.1	8.42	47.1	40.7	11.2	0.048
A10	11	43.9	40.4	13.3	5.74	43.3	40	12.6	9.96	67.3	51.9	14.3	8.34	54.8	43.6	11.9	0.061
A11	7.33	41.6	28	9.07	5.5	41	27.4	8.7	10.5	63.7	54.7	14.7	10.2	61.1	51	14.3	0.069
A12	7.3	44.2	30.1	9.88	5.61	43.8	29.8	9.23	7.66	50.6	30	11.1	6.86	47.3	35	10.2	0.071
0°	Ra	Ry	Rz	Rq	Ra	Ry	Rz	Rq	Ra	Ry	Rz	Rq	Ra	Ry	Rz	Rq	
A1	8.02	34.6	31	9.13	7.81	33.2	30	8.89	10.2	55	47.9	13	7.1	42.2	35.5	9.2	0.096
A2	6.64	38.6	29.7	8.34	5.97	34.4	24	7.42	10.4	55.5	49.6	13.4	8.8	49.5	42.2	11.4	0.094
A3	7.77	41	31.8	9.01	7.09	40.2	31.4	8.68	9.36	53.7	43.4	11.8	8.2	47.5	40.2	10.8	0.048
A4	7.38	44.1	34	9.24	6.65	43.7	33.5	8.77	7.89	45.6	42.6	12.7	6.7	41.6	35.6	8.9	0.061
A5	6.07	37.8	25.9	7.56	5.33	37.4	25.4	7.15	7.63	43.3	37	10.8	5.9	41	31.4	8.2	0.048
A6	6.22	41.3	32.1	8.14	5.64	40.7	31.4	7.73	8.82	50.7	40.1	11	7.4	48.4	37.1	10	0.066
A7	6.64	38.6	29.7	8.34	5.82	35.9	23.8	7.49	12.6	66.4	57.3	16.1	7.6	49	37.7	10.4	0.053
A8	6.46	35.1	26.6	7.81	6.05	34.6	26	7.33	11	45	40	12.1	7.5	48.1	36.2	10.1	0.055
A9	7.82	44.9	31.9	9.85	7.03	44.5	31.5	9.3	7.45	41.3	34.7	11.8	6.5	40.5	33.8	8.6	0.048
A10	6.02	41.8	28.8	8.19	5.34	40	26	7.19	8.71	45.2	38	12.4	6.8	41.4	33.8	8.9	0.059
A11	6.59	38.3	27.8	8.09	5.98	37.7	27.3	7.69	7.13	40.1	37.4	12.4	6	38.4	35.4	8.2	0.078
A12	6.99	36.6	28.5	8.4	6.41	36	27.8	8.03	8.41	44.9	36.7	13	6.6	42.2	35.7	9	0.074

The specimens were tested under two levels of normal load, 39.24 N and 58.86 N, as well as two sliding velocities, 15 mm/s and 20 mm/s. Based on the active contact area of 162 mm^2, the corresponding nominal contact pressures were approximately 0.247 MPa and 0.370 MPa. This range effectively covers contact conditions representative of engineering applications involving polymer-based tribological pairs.

3. Results

3.1. Surface Topography Before and After Testing

The initial surface roughness of the FFF-printed polycarbonate specimens exhibited clear anisotropy as a function of build orientation. Specimens printed at 90° showed longitudinally aligned filament paths with minimal step-over irregularities, while the 45° and 0° orientations displayed increasingly pronounced transverse features.

Similar orientation-dependent surface anisotropy and its influence on tribological response have been investigated for additively manufactured polymer systems. Previous studies on 3D-printed polymers have demonstrated that build orientation governs the alignment of filament tracks, surface roughness evolution, and local contact mechanics,

which in turn directly affect friction stability and wear mechanisms under reciprocating sliding conditions [36–38].

Representative 2D profiles of the printed surfaces were measured before and after the testing on the tribometer. All measured surface roughness parameters are shown in Table 7. Figure 5 shows the 2D profiles of the pin and plate specimens, which were printed at 90° before and after the testing under different conditions.

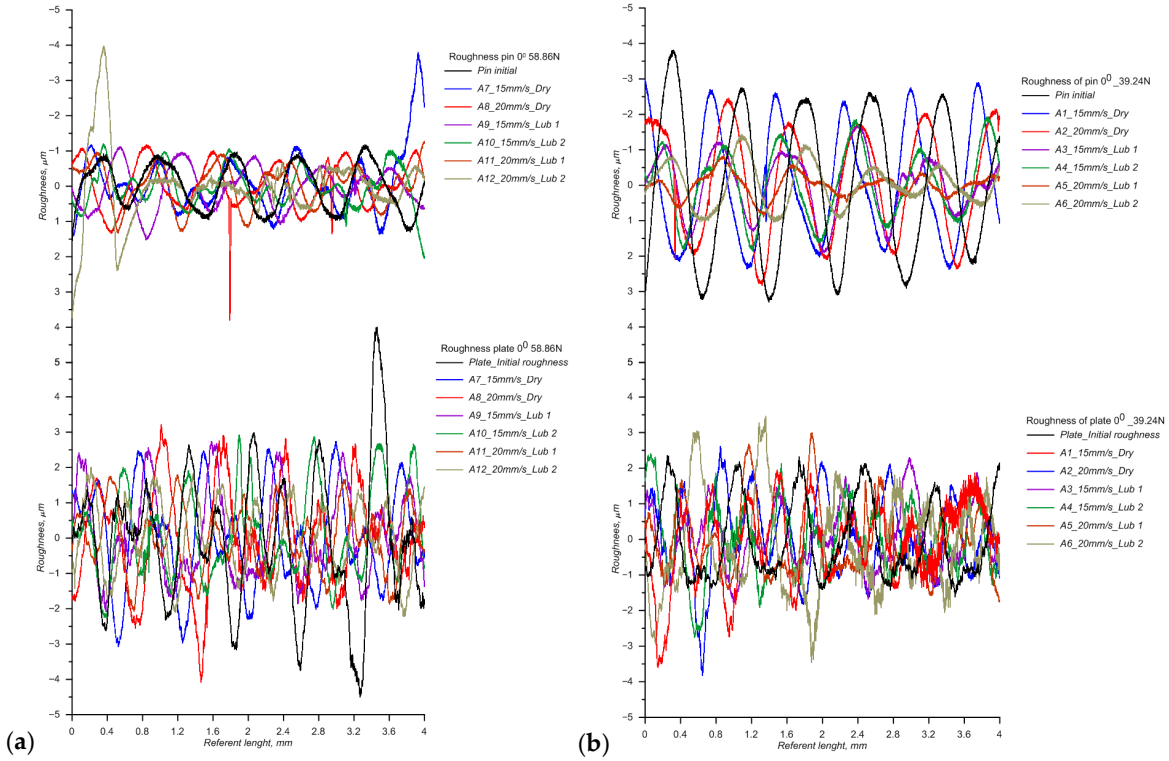

Figure 5. Surface profiles of pin and plate specimens loaded with: (**a**) 39.24 N; (**b**) 58.86 N.

In Figure 5, (a) shows surface profiles of the pin and plate specimens loaded with 39.24 N, while (b) shows the specimens loaded with 58.86 N.

In Figure 6, the 2D profiles of the pin and plate printed at 45° are shown.

In Figure 6, (a) shows surface profiles of the pin and plate specimens loaded with 39.24 N, while (b) shows the specimens loaded with 58.86 N.

In Figure 7, the 2D profiles of the pin and plate printed at 0° are shown.

In Figure 7, (a) shows surface profiles of the pin and plate specimens loaded with 39.24 N, while (b) shows the specimens loaded with 58.86 N.

A detailed analysis of the measured surface roughness profiles reveals stable tribological behavior of polycarbonate under low and medium normal loads. This can be attributed to the influence of elastoplastic deformation, which provides polycarbonate with exceptional resistance to localized asperity damage. It can be concluded that, under low and medium normal loads, polycarbonate develops a wide zone of plastic deformation that redistributes stresses, protects surface peaks from micro-fracture, and results in a more stable friction coefficient during long sliding cycles. This behavior is consistent with previously published results for tribological responses of amorphous and semi-amorphous polymers, where elastoplastic deformation dominates over brittle fracture, enabling stress redistribution and suppression of severe asperity damage during sliding [39,40].

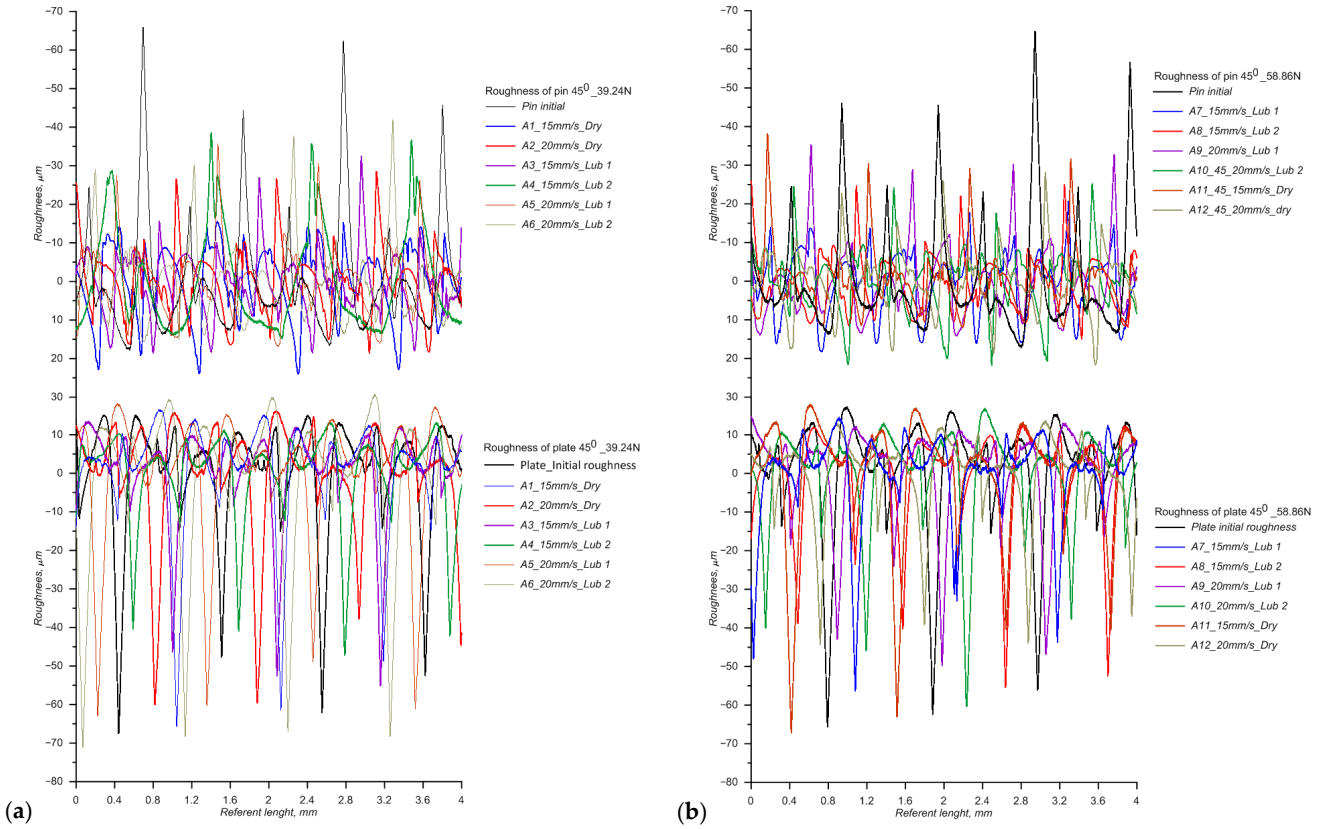

Figure 6. Two-dimensional surface profiles on 45° due to: (**a**) 39.24 N; (**b**) 58.86 N.

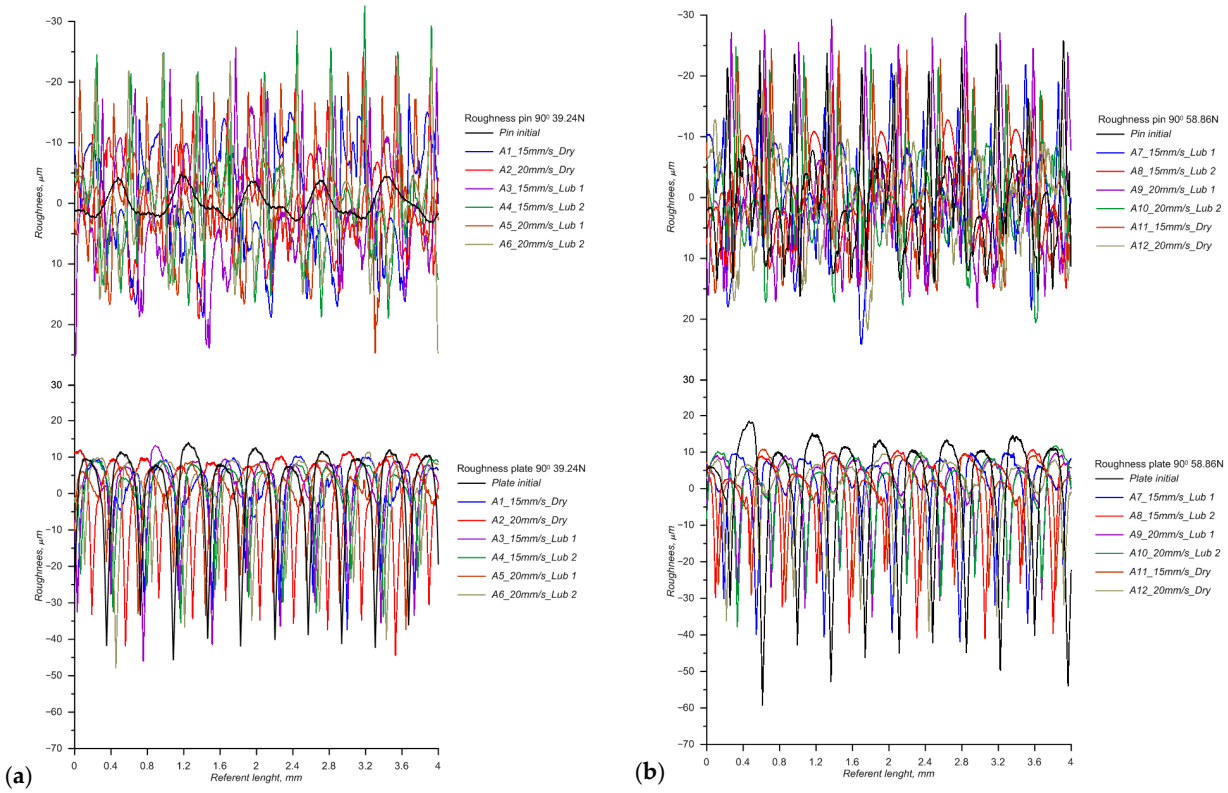

Figure 7. Two-dimensional surface profiles on 0° due to: (**a**) 39.24 N; (**b**) 58.86 N.

By examining the diagrams in Figure 5a,b for the 90° orientation, it is clearly visible that the surface roughness profiles of the contacting samples remain close to their initial state. The amplitude variations are small, symmetric, and significantly less sensitive to increases in normal load. This behavior is associated with the 90° printing orientation, which provides the highest structural stiffness in the normal direction, allowing for uniform load distribution. In both cases, lubricants improve the stability of the profiles, but the effect is more pronounced in Figure 5b, particularly for Lub 2, where transfer film formation and the higher effective viscosity under load more efficiently fill micro-valleys.

Based on the diagrams in Figure 6, pronounced changes in surface roughness are visible for samples printed at 45°. The initial roughness profiles (black line) contain asperities of approximately 20–25 μm and valleys reaching −70 μm on both the pin and plate surfaces. After tests conducted under a normal load of 39.24 N, at sliding speeds of 15 mm/s and 20 mm/s, and under different lubrication regimes (dry, Lub 1, Lub 2), the profiles show a reduction in the valley depth $\boldsymbol{R_v}$ and partial preservation of the peak height $\boldsymbol{R_p}$. This can be explained by the amorphous structure of PC and the elastoplastic deformation mechanism: under load, the material at the asperity peaks does not fracture in an abrasive manner but instead flows plastically and partially fills the deeper zones of the surface. The presence of Lub 1 and Lub 2 further promotes transfer film formation and micro-valley filling, producing the observed reduction in $\boldsymbol{R_v}$ compared to dry conditions. In the dry regime, the valleys diminish more slowly. From the profiles in Figure 6a,b, it is evident that the valleys $\boldsymbol{R_v}$ on the pin surface are significantly reduced compared to those on the plate. This is a consequence of the non-uniform distribution of contact stresses and the more intensive elastoplastic deformation occurring at the asperities of the pin. Due to its smaller real contact area and constant dynamic loading, the pin exhibits more pronounced plastic material flow. The plate, with a larger load-bearing surface and lower contact pressures, shows a more moderate level of deformation and micro-valley filling. Comparable reductions in valley depth and stabilization of friction due to plastic flow and transfer film formation in inclined or off-axis printing orientations have been reported for FFF-printed PLA, PC, and composite systems tested under similar reciprocating conditions [36,37,39].

By comparing Figure 6a,b, it is evident that higher normal loads induce more intensive shearing and plastic flow of the material. At 58.86 N, the valleys $\boldsymbol{R_v}$ become much shallower and the profile curves smoother, indicating more efficient filling of micro-depressions.

For the 0° FFF-printing orientation (Figure 7a,b), the initial surface roughness profile lines are aligned with the sliding direction and dominated by long wavelength components typical of parallel filament tracks. After tests at 39.24 N, the pin exhibits short-wavelength roughness components and the largest deviation from the initial surface profile, indicating micro-grooving along the filament direction. Sliding occurs along continuous ridges, while the load is distributed across multiple parallel micro-contacts, resulting in significant deformation even at relatively low load levels. Lubricants mitigate, but do not completely eliminate the short-wavelength roughness component, consistent with their rheological behavior. Lub 1, with higher low-shear viscosity and more pronounced shear-thinning at higher sliding speeds, more effectively fills surface valleys, whereas Lub 2 maintains a more stable lubricant film under load due to its more uniform viscosity–shear rate response. This explains why the profiles stabilize in the presence of lubricants, although the micro-grooving mechanism persists.

The literature indicated that printing orientations aligned parallel to the sliding direction often promote micro-grooving and directional deformation due to continuous ridge–asperity interaction, leading to higher friction levels and delayed transition toward

mixed lubrication regimes. Such behavior has been consistently observed in polymer–polymer and polymer–metal contacts produced by additive manufacturing [37,38,40].

In contrast, the plate retains the valley structure of the initial roughness profile, with moderate $\boldsymbol{R_p}$ reduction and slight filling of $\boldsymbol{R_v}$, which is attributed to the favorable distribution of normal loads across a larger contact area and reduced levels of local shear deformation. At 58.86 N, the observed trends become more pronounced but do not change the fundamental behavior of either sample. The pin exhibits a more stable profile under lubrication, with reduced micro-valleys. The rheological characteristics of the lubricants indicate that Lub 1, due to its higher viscosity at low shear rates, more effectively fills micro-depressions under higher normal load, whereas Lub 2 maintains a stable film during speed variations. The plate shows more intensive peak reduction compared to its initial roughness profile with increasing load.

3.2. Rheological Behavior of Lubricants

Yield stress was determined as an indicator of the minimal stress required for the lubricant to transition from a solid-like to a liquid-like regime, thereby enabling assessment of its stability and ability to retain shape before flow initiation.

Oscillatory tests were conducted to determine the storage modulus and loss modulus, which represent fundamental parameters for assessing the internal structure of the used lubricants. The obtained viscosity is given in Figure 8.

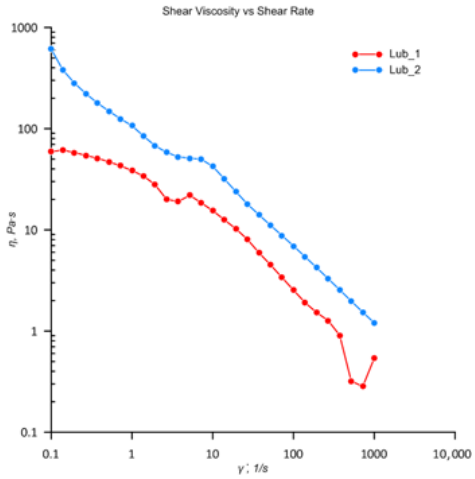

Figure 8. Rheological analysis of Lub 1 and Lub 2 viscosity.

Both lubricants displayed a characteristic decrease in viscosity with increasing shear rate, indicating pseudoplastic (shear-thinning) behavior typical of technical greases and gel-type lubricants. For the acid-free petrolatum (Lub 2), the measured viscosity values were considerably higher across the entire range of observed shear rates, but its viscosity decreased with increasing shear, further indicating a pronounced shear-thinning effect and a more sensitive internal structure. The silicone paste (Lub 1) exhibited a more gradual viscosity decrease, while Lub 2 maintained higher viscosity levels across the investigated shear-rate range, favoring more stable film persistence under load. These rheological findings have a direct influence on the tribological behavior of the PC–PC contact. Specifically, Lub 1 more effectively fills micro-irregularities at lower sliding speeds, whereas Lub 2 provides a more stable lubricant film throughout the entire testing cycle. Both lubricant-obtained parameters are given in Table 8.

Table 8. Measured rheological lubricant parameters.

Lub 1			Lub 2		
τ_1, Pa	$\dot{y}_1$, 1/s	η_1, Pa·s	τ_2, Pa	$\dot{y}_2$, 1/s	η_2, Pa·s
5.932	0.1	59.32	61.098	0.1	610.98
85.337	0.139	613.9353	52.865	0.139	380.3237
11.222	0.193	58.14508	54.656	0.193	283.1917
14.610	0.268	54.51493	59.527	0.268	222.1157
19.001	0.373	50.94102	66.935	0.373	179.4504
24.381	0.518	47.06757	77.175	0.518	148.9865
30.899	0.72	42.91528	90.206	0.72	125.2861
38.560	1	38.56	106.88	1	106.88
47.287	1.39	34.01942	117.34	1.39	84.41727
53.918	1.93	27.93679	130.89	1.93	67.81865
53.678	2.68	20.0291	156.38	2.68	58.35075
71.013	3.73	19.03834	196.45	3.73	52.66756
113.71	5.18	21.95174	264.77	5.18	51.1139
133.17	7.2	18.49583	359.13	7.2	49.87917
154.62	10	15.462	424.01	10	42.401
174.88	13.9	12.58129	443.22	13.9	31.88633
197.91	19.3	10.2544	461.16	19.3	23.8943
216.28	26.8	8.070149	482.56	26.8	18.00597
221.64	37.3	5.942091	525.3	37.3	14.08311
233.9	51.8	4.515444	575.66	51.8	11.11313
243.23	72	3.378194	632.43	72	8.78375
253.48	100	2.5348	692.77	100	6.9277
265.45	139	1.909712	753.65	139	5.421942
294.32	193	1.524974	817.47	193	4.235596
341.08	268	1.272687	883.16	268	3.295373
338.11	373	0.906461	952.13	373	2.552627
165.65	518	0.319788	1025.8	518	1.980309
204.27	720	0.283708	1105.3	720	1.535139
539.97	1000	0.53997	1203.3	1000.00	1.2033

The obtained results enabled a comprehensive evaluation of viscosity, viscoelastic response, and stability of the used lubricants, thereby providing a scientifically substantiated basis for understanding their behavior under real-world operating conditions, as well as for further formulation development and material optimization.

3.3. Coefficient of Friction (COF) Under Different Conditions

The coefficient of friction (COF) was evaluated under four distinct operating conditions determined by the combination of applied normal load (4 kg = 39.24 N, 6 kg = 58.86 N) and reciprocating sliding velocity (15 mm/s and 20 mm/s). For each condition, the effect of printing orientation (0°, 45°, 90°) was examined. The corresponding COF evolution curves are presented in Figures 9–12. Orientation-dependent trends in COF evolution observed in this study are in good agreement with the previous literature results on additively manufactured polymers, where surface texture anisotropy and filament orientation were identified as key parameters controlling friction magnitude and stability under boundary-dominated sliding conditions [37,38].

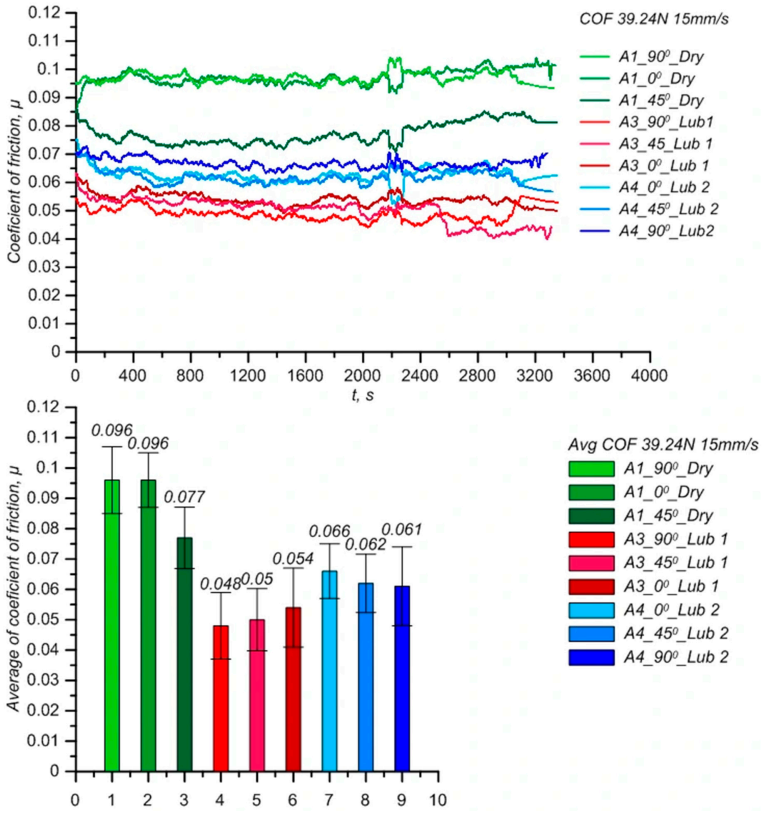

Figure 9. COF at lower load and lower speed (39.24 N, 15 mm/s).

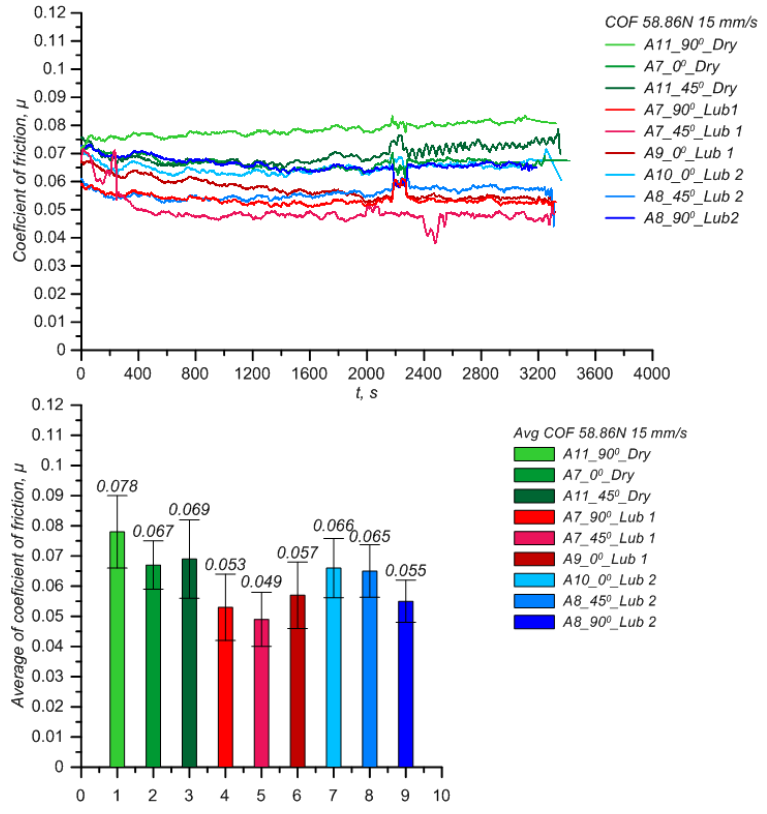

Figure 10. COF at higher load and lower speed (58.86 N, 15 mm/s).

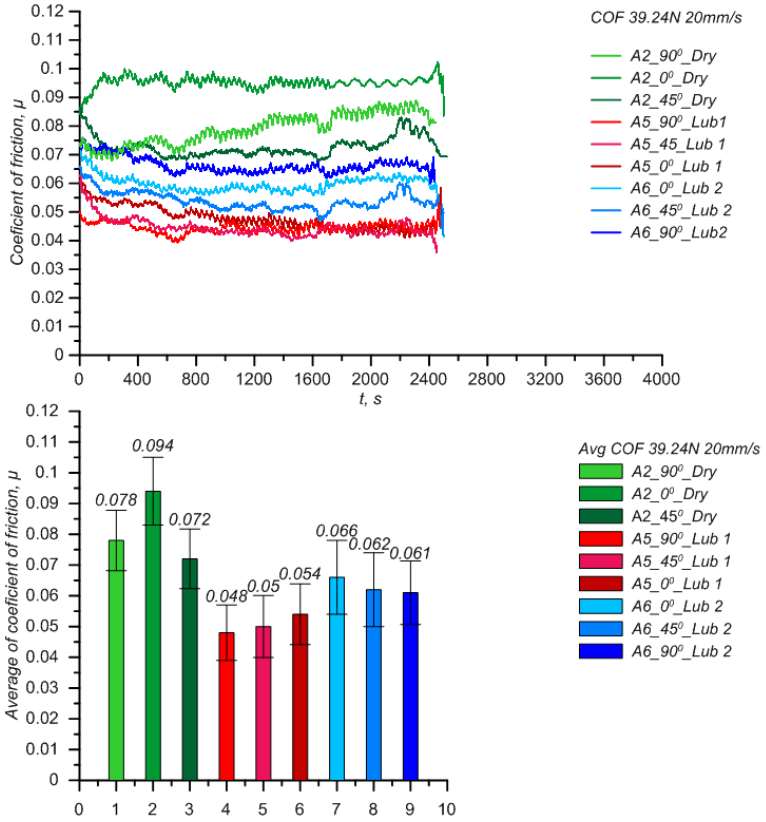

Figure 11. COF at lower load and higher speed (39.24 N, 20 mm/s).

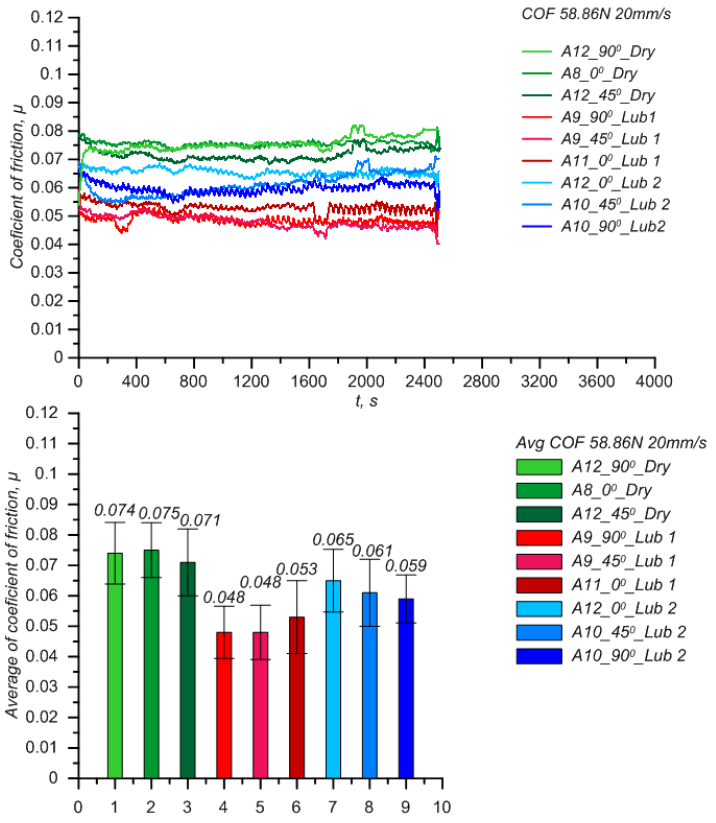

Figure 12. COF at higher load and higher speed (58.86 N, 20 mm/s).

3.3.1. COF at Lower Load and Lower Speed (39.24 N, 15 mm/s)

Under the lowest load–speed combination, the frictional response was dominated by asperity-controlled interactions. The 45° orientation exhibited the lowest mean COF and the most stable time-dependent behavior, resulting from longitudinal filament alignment that minimizes asperity interlocking. The 0° orientation showed moderate COF fluctuations due to diagonal ridge engagement, while the 90° orientation produced the highest COF and the greatest instability.

At low load and low speed, hydrodynamic and even mixed lubrication effects were negligible in all cases, and the contact remained fully within the boundary regime. Similar findings, where inclined printing orientations provide reduced asperity interlocking and improved friction stability compared to transverse orientations, have been reported for FFF-printed PLA, ABS, and PC materials tested under low-load and low-speed conditions [37,40].

3.3.2. COF at Higher Load and Lower Speed (58.86 N, 15 mm/s)

Increasing the load from 39.24 N to 58.86 N while maintaining the same sliding speed resulted in a slight reduction in COF for all orientations. This behavior is attributed to increased real contact area and partial softening of the polymer surface, which reduced micro-asperity interference.

Nevertheless, the orientation-dependent trends changed slightly: 45° yielded the lowest mean COF under this condition, 0° showed intermediate values with moderate fluctuations, while 90° remained the highest due to transverse ridges.

3.3.3. COF at Lower Load and Higher Speed (39.24 N, 20 mm/s)

Increasing the sliding velocity to 20 mm/s at the lower load produced a noticeable decrease in COF for all orientations. Higher speed improved lubricant entrainment (in lubricated tests) and reduced stick–slip effects (in dry tests), resulting in smoother frictional traces.

The reduction was most pronounced in the 90° and 45° samples, indicating enhanced alignment between the sliding direction and the surface texture. The 0° specimens still exhibited the highest COF, but the amplitude of fluctuations was lower compared to the 15 mm/s case.

3.3.4. COF at Higher Load and Higher Speed (58.86 N, 20 mm/s)

The combination of higher load and higher sliding velocity produced the lowest COF values overall. Both effects of load-induced softening and velocity-enhanced lubricant entrainment contributed to reduced asperity interaction.

Under these conditions, all orientations approached early mixed lubrication behavior in the lubricated tests, though boundary friction still dominated in the dry regime. The 45° orientation again provided the most favorable frictional performance, while the 90° orientation showed the slowest transition toward reduced friction.

3.4. Stribeck Curve and Lubrication Regime Identification

The Stribeck parameter is determined by Equation (2).

$$S = \frac{\eta_{eff} \cdot v}{p} \quad (2)$$

where S—Stribeck parameter (unitless), η_{eff}—effective dynamic viscosity of lubricant Pa·s, v—sliding velocity m/s, and p—contact pressure Pa.

The Stribeck parameter was calculated for all lubricated conditions using temperature-corrected viscosity values obtained from rheological testing.

The resulting Stribeck parameters (Figure 13) demonstrate that the PC–PC contact operates primarily within the boundary and early mixed lubrication regimes, consistent with low velocities and soft polymer surfaces.

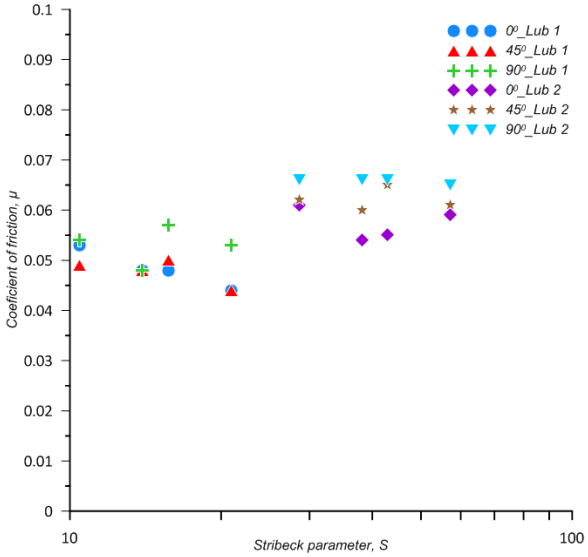

Figure 13. Stribeck curves.

Key findings that can be seen from the Stribeck curves include the following:

- the 45° orientation shifts the curve toward lower COF due to smoother lubricant flow;
- the 0° orientation delays entry into mixed lubrication due to asperity-dominated contact;
- Lub 2 provides a smoother transition because of stable viscosity;
- Lub 1 remains longer in the boundary regime due to its sharp viscosity decay.

These results confirm that surface anisotropy, lubricant rheology, and applied load jointly determine lubrication regime transitions in FFF-printed PC–PC contacts.

The combined influence of surface anisotropy, lubricant rheology, and load-dependent deformation observed in the present Stribeck analysis is consistent with tribological models and experimental results from the literature [39,40] for additively manufactured polymer contacts operating in boundary and early mixed lubrication regimes.

4. Discussion

The tribological behavior of FFF-printed polycarbonate was strongly governed by the combined effects of layer orientation, surface-topography evolution, applied load, sliding velocity, and lubricant rheology. The results confirm that polymer–polymer contacts under low loads (39.24–58.86 N) and low velocities (15–20 mm/s) operate predominantly within the boundary lubrication regime, consistent with previous observations for soft polymers and greases in reciprocating motion [23,27].

4.1. Influence of Layer Orientation and Surface Topography

The initial roughness measurements demonstrated strong anisotropy, with the 45° orientation showing smoother longitudinal filament alignment, while 0° and 90° presented more pronounced transverse features. After testing, 45° and 90° samples exhibited mostly plastic smoothing, whereas 0° samples developed clear wear tracks and asperity removal, in agreement with adhesive and mild abrasive mechanisms. These trends correlate with

prior findings that surface orientation controls asperity interlocking and debris formation in FFF parts.

The comparative analysis of surface roughness for all tested orientations, 90°, 45°, and 0°, clearly shows that the microstructure formed during FFF printing has a decisive influence on how surface topography evolves during reciprocating sliding. For the 0° orientation, where the filament paths are parallel to the sliding direction, the dominant mechanisms are shear and micro-grooving. Although the lubricants fill micro-depressions, the surface still exhibits pronounced $\boldsymbol{R_v}$ values due to sliding along continuous ridges. In this regard, the 0° orientation can be considered the most sensitive to the development of short-wavelength micro-roughness, even though the global geometry remains stable.

In the case of the 45° orientation, a combination of longitudinal shearing and transverse cutting of asperity peaks occurs, but much less than expected. This means that the 45° orientation represents the geometry with the largest surface transformation of asperities and the most pronounced plastic deformation. Lubricants have the strongest effect in this orientation, as the viscosity and shear-thinning behavior of the applied lubricants facilitate easier filling of surface irregularities, especially under higher normal loads.

In contrast to the 0° orientations, the 90° and 45° orientations exhibit the most stable behavior under all testing conditions. This is because the normal load is transmitted perpendicular to the sliding direction and through the structurally stiffest cross-section of the material. This indicates that the 90° and 45° orientations are more resistant to wear and changes in surface roughness under low and medium normal loads.

The strong orientation-dependent behavior is reflected directly in the COF curves:

- The 45° orientation consistently provided the lowest COF in most regimes (except 58.86 N on the 15 mm/s regime), due to minimized asperity interference and favorable lubricant entrainment pathways.
- The 0° orientation produced the highest COF, since transverse ridges acted as mechanical barriers and promoted boundary-dominated sliding.
- The 90° samples showed transitional behavior, combining characteristics of both aligned and misaligned filament structures.

These results reinforce earlier studies on anisotropic friction in additively manufactured polymers but extend them to lubricated PC–PC contacts, which remain scarcely represented in the literature.

Additional post-test surface images obtained by optical microscopy (Figure 14) further support the proposed orientation-dependent wear mechanisms.

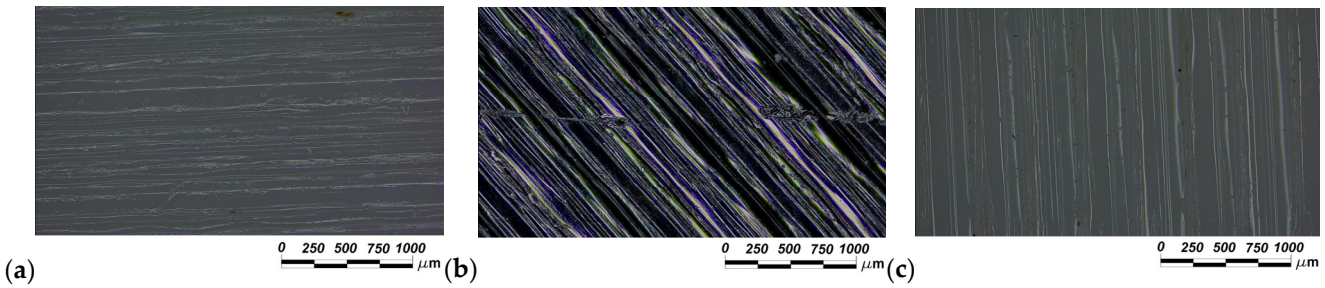

(**a**) (**b**) (**c**)

Figure 14. Worn surface: (**a**) Sample A12 90°; (**b**) Sample A12 45°; (**c**) Sample A12 0°.

The 90° orientation exhibits predominantly smooth and continuous wear tracks, indicating stable sliding conditions and uniform load distribution. In the case of the 45° orientation, pronounced asperity smoothing and evidence of plastic flow are observed, consistent with reduced friction and enhanced lubricant interaction. In contrast, the 0° orientation reveals distinct micro-grooving aligned with filament tracks, confirming asperity-

dominated contact and explaining the higher friction levels and delayed transition toward mixed lubrication regimes.

4.2. Effect of Load and Sliding Velocity on COF

Across all orientations, increasing the normal load from 39.24 N to 58.86 N caused a modest reduction in COF. This counterintuitive but well-documented phenomenon arises from load-induced real-area increase, which reduces localized stress and smooths micro-asperity motion. Similarly, increasing sliding velocity from 15 to 20 mm/s reduced COF by lowering stick–slip intensity and increasing lubricant entrainment (where applicable).

The superposition of mechanical (load-driven) and kinematic (velocity-driven) effects demonstrates that even small changes in operating conditions significantly alter frictional stability in polymer contacts. These insights are critical for engineering sliding bushings, guides, and low-load reciprocating mechanisms.

4.3. Rheological Effects of Lubricants on COF

Since the experimental investigations were conducted in the boundary lubrication regime at low sliding speeds and low normal loads, and considering the obtained rheological results for lubricants Lub 1 and Lub 2, it can be observed that the COF exhibited the lowest values in all tests under lubrication with Lub 1. This indicates that the COF does not depend directly on the viscosity of the lubricant, but rather on its chemical composition and its ability to form a protective film. Although Lub 2 demonstrates more stable viscosity, Lub 1 consistently achieves lower COF values across all testing conditions. The reason is that Lub 1 exhibits higher adhesiveness to PC surfaces, fills micro-irregularities more effectively, and forms an effective boundary protective layer that reduces direct asperity interaction. In contrast, despite its more stable rheological behavior, Lub 2 adheres less effectively to PC surfaces and is more easily squeezed out of the contact zone, which consequently results in higher COF.

These findings confirm that grease-like media with stable polymeric networks (silicone-based) support more uniform lubrication in PC–PC contacts.

4.4. Stribeck Behavior and Regime Identification

Based on viscosity-corrected Stribeck parameters, all greased contacts operated within the boundary and early mixed lubrication regions, aligning with expectations for soft polymers, low velocities, and limited hydrodynamic film thickness. Notably:

- The 90° orientation shifted Stribeck curves downward, indicating improved film formation and reduced friction.
- The 0° orientation displayed a delayed transition, reflecting asperity-dominated sliding.
- Lub 2 lubricant produced smoother Stribeck curves, while Lub 1 maintained boundary behavior longer.

These combined results confirm that lubrication regime transitions in additively manufactured polymers depend jointly on surface orientation, material compliance, and lubricant rheology—a relationship largely missing in the existing literature.

If, as well the temperature is taken into consideration, given that the experiments were performed at room temperature (22 $\pm$ 3 °C), which is far below the Vicat Softening Temperature (VCT $\approx$ 119 °C) and the glass transition temperature (Tg $\approx$ 145 °C), it can be concluded that no changes occur in the molecular arrangement of PC and that no thermal softening takes place, which further stabilizes friction and wear.

After the tribological tests under all load, speed, and lubrication conditions, a reduction in the valley depth $\boldsymbol{R_v}$ can be observed.

4.5. Contribution to Research Gap

The present study addresses multiple gaps identified in the introduction:

1. Lack of data on lubricated PC–PC contacts

The work provides one of the first systematic datasets combining dry and greased PC–PC sliding under reciprocating motion.

2. Missing correlation between layer orientation, roughness evolution, and friction

The study directly links anisotropic surface changes to frictional response across four operating regimes.

3. Limited integration of tribology and rheology

By combining rheometry with Stribeck analysis, the work offers a unified understanding of how grease viscosity, temperature sensitivity, and shear-thinning govern lubrication in polymer–polymer sliding.

Overall, the discussion highlights that the interaction between FFF microstructure, lubricant behavior, and operating conditions plays a central role in dictating friction performance.

5. Conclusions

This study provides a comprehensive evaluation of the tribological and rheological behavior of FFF-printed polycarbonate under varying layer orientations, loads, velocities, and lubrication conditions. Based on the experimental findings, the following conclusions can be drawn:

- Layer orientation is the dominant factor controlling friction behavior.
  The 45° and 90° orientations yielded the lowest COF and mildest wear, while 0° produced the highest friction and most severe asperity disruption.
- Surface topography evolution strongly depends on filament alignment.
  Longitudinally printed surfaces (90°) deform plastically, whereas transverse layers (0°) exhibit adhesive and abrasive wear patterns.
- Moderate increases in load and sliding velocity reduce COF.
  Higher loads reduce asperity interference through increased real contact area, while higher velocities diminish stick–slip and improve lubrication.
- Lubricant rheology plays a decisive role in friction regulation.
  Lub 1 shows steep viscosity decay and boundary-dominated behavior, while Lub 2 maintains stable viscosity and supports smoother friction reduction.
- Stribeck analysis confirms the boundary to early mixed lubrication.
  No transition to full hydrodynamic regime was observed, consistent with soft polymer surfaces and low velocities.
- The results bridge important research gaps.
  This work integrates tribological performance, surface evolution, and rheology for PC–PC contacts—a combination rarely reported in the current AM literature.
- This work holds practical relevance.

As a consequence of the low and medium normal loads applied at low sliding speeds, polycarbonate exhibits negligible degradation of its tribological characteristics, which makes it suitable for use in FFF-printed sliding guides, electronic components, medical devices, and various robotic mechanisms—fully consistent with the results presented in this study.

From a practical engineering perspective, the results of this study provide direct guidelines for the design and application of FFF-printed polycarbonate sliding components. The findings demonstrate that print orientation should be selected based on the dominant loading and sliding direction: the 45° orientation offers the most favorable compromise

between low friction and surface stability, while the 0° orientation ensures robust and stable behavior under repeated loading. In contrast, the 90° orientation should be avoided in applications involving continuous sliding parallel to filament tracks due to increased micro-grooving and higher friction. These recommendations are directly applicable to the design of low-load sliding guides, bushings, positioning mechanisms, and polymer-based tribological pairs in automated and mechatronic systems.

The findings are directly applicable to low-load reciprocating mechanisms, guides, biomedical components, and consumer-product sliding interfaces made from 3D-printed PC. Further investigations should include 3D topographic evolution mapping during sliding and advanced lubrication models incorporating temperature-dependent viscosity and polymer compliance to deepen understanding of lubrication transitions in additively manufactured polymer systems. Future work will also include the possibility of the use of biolubricants in polymer contacts.

Author Contributions: Conceptualization, M.M. (Miloš Matejić) and M.B.; methodology, M.M. (Marija Matejić); software, J.M.; validation, D.R.; formal analysis, J.S. and M.M. (Marija Matejić); experiment preparation, J.M.; investigation, M.M. (Marija Matejić); resources, N.J.; data curation, M.M. (Marija Matejić); writing—original draft preparation, M.M. (Miloš Matejić); writing—review and editing, M.B.; visualization, M.M. (Marija Matejić); supervision, M.B. and M.M. (Miloš Matejić); project administration, D.R.; funding acquisition, M.M. (Miloš Matejić) All authors have read and agreed to the published version of the manuscript.

Funding: This research received no external funding. The whole investigation is funded by the authors.

Data Availability Statement: The original contributions presented in this study are included in the article. Further inquiries can be directed to the corresponding author.

Conflicts of Interest: The authors declare no conflicts of interest.

Abbreviations

The following abbreviations are used in this manuscript:

AM	Additive manufacturing
FFF	Fused filament fabrication
PC	Polycarbonate
COF	Coefficient of friction
Lub 1	Acid-free technical petrolatum lubricant
Lub 2	Silicone insulating paste lubricant
VCT	Vicat softening temperature
Tg	Glass transition temperature

References

1. Holmberg, K.; Erdemir, A. Influence of tribology on global energy consumption, costs and emissions. *Friction* **2017**, *5*, 263–284. [CrossRef]
2. Sasaki, S. Environmentally Friendly Tribology (Eco-Tribology). *J. Mech. Sci. Technol.* **2010**, *24*, 67–71. [CrossRef]
3. Brostow, W. Tribology of Polymers. *J. Mater. Educ.* **2010**, *32*, 273–290.
4. Bahar, A.; Belhabib, S.; Guessasma, S.; Benmahiddine, F.; Hamami, A.E.A.; Belarbi, R. Mechanical and Thermal Properties of 3D Printed Polycarbonate. *Energies* **2022**, *15*, 3686. [CrossRef]
5. Stoimenov, N.; Kandeva, M.; Zagorski, M.; Panev, P. Static and Kinetic Friction of 3D Printed Polymers and Composites. *Tribol. Ind.* **2024**, *46*, 97–106. [CrossRef]
6. Singh, S.; Ramakrishna, S.; Singh, R. Material Issues in Additive Manufacturing: A Review. *J. Manuf. Process.* **2017**, *25*, 185–200. [CrossRef]
7. Kershah, T.; Looijmans, S.F.S.P.; Anderson, P.D.; van Breemen, L.C.A. Temperature Dependent Two-Body Abrasive Wear of Polycarbonate Surfaces. *Wear* **2019**, *440–441*, 203089. [CrossRef]

8. Carrión, F.J.; Arribas, A.; Bermúdez, M.-D.; Guillamon, A. Physical and Tribological Properties of a New Polycarbonate-Organoclay Nanocomposite. *Eur. Polym. J.* **2008**, *44*, 968–977. [CrossRef]
9. Norani, M.; Chua, M.I.H.; Abdollah, M.F.B.; Amiruddin, H.; Ramli, F.; Tamaldin, N. Mechanical and Tribological Properties of FFF 3D-Printed Polymers: A Brief Review. *J. Tribol.* **2021**, *29*, 11–30.
10. Dangnan, F.; Espejo, C.; Liskiewicz, T.; Gester, M.; Neville, A. Friction and Wear of Additive-Manufactured Polymers in Dry Contact. *J. Manuf. Process.* **2020**, *59*, 238–247. [CrossRef]
11. Turek, P.; Bazan, A.; Bulicz, M. Effect of 3D Printing Orientation on the Accuracy and Surface Roughness of Polycarbonate Samples. *Machines* **2025**, *13*, 9. [CrossRef]
12. Hanon, M.M.; Kovács, M.; Zsidai, L. Tribology Behaviour Investigation of 3D Printed Polymers. *Int. Rev. Appl. Sci. Eng.* **2019**, *10*, 173–181. [CrossRef]
13. Mergler, Y.J.; Kampen, R.J.; Nauta, W.J.; Schaake, R.P.; Raas, B.; Griensven, J.G.H.; Meesters, C.J.M. Influence of Yield Strength and Toughness on Friction and Wear of Polycarbonate. *Wear* **2005**, *258*, 915–923. [CrossRef]
14. Mandal, S.; Sain, P.K.; Kabra, A.; Reger, N.C.; Solanki, D.; Goyal, R.K.; Bhargava, A.K. Tribological Behavior of Silicon Nitride Reinforced Polycarbonate Nanocomposites. *J. Appl. Polym. Sci.* **2023**, *140*, e53807. [CrossRef]
15. Grenadyorov, A.S.; Yuriev, Y.N.; Solovyev, A.A.; Runts, A.A.; Oskomov, K.V.; Semenov, V.A.; Sypchenko, V.S. Mechanical and Tribological Properties of Diamondlike Carbon-Coated Polycarbonate. *J. Vac. Sci. Technol. A* **2023**, *42*, 10402. [CrossRef]
16. Jezny, T.; Mital, G.; Spisak, E.; Gajdos, I. Research of the Resistance of Polycarbonate Samples Made By Fdm Technology To Abrasive Action. *MM Sci. J.* **2024**, *2024*, 8026–8032. [CrossRef]
17. Difallah, B.; Kharrat, M.; Dammak, M.; Monteil, G. Improvement in the Tribological Performance of Polycarbonate via the Incorporation of Molybdenum Disulfide Particles. *Tribol. Trans.* **2014**, *57*, 806–813. [CrossRef]
18. Wang, Y.; Guan, W.; Fischer, C.; Wehner, S.; Dang, R.; Li, J.; Guo, W. Microstructures, Mechanical Properties and Tribological Behaviors of Amorphous Carbon Coatings in-Situ Grown on Polycarbonate Surfaces. *Appl. Surf. Sci.* **2021**, *557*, 149791. [CrossRef]
19. Özdemir, T.; ÖGE, M. Prediction of Tribological Properties of PC-PBT/GNP-MWCNT Nanocomposites Using Machine Learning Models. *J. Appl. Polym. Sci.* **2025**, *142*, e56834. [CrossRef]
20. Patel, J.R.; Chauhan, K.V.; Rawal, S.; Patel, N.P.; Subhedar, D.G. Advances and Challenges in Bio-Based Lubricants for Sustainable Tribological Applications: A Comprehensive Review of Trends, Additives, and Performance Evaluation. *Lubricants* **2025**, *13*, 440. [CrossRef]
21. Berman, D. Plant-Based Oils for Sustainable Lubrication Solutions—Review. *Lubricants* **2024**, *12*, 300. [CrossRef]
22. Lin, Z.; Wang, F.; Gao, D.; Ba, D.; Liu, C. Frictional and Optical Properties of Diamond-like-Carbon Coatings on Polycarbonate. *Plasma Sci. Technol.* **2013**, *15*, 690–695. [CrossRef]
23. Cann, P. Lubrication Mechanisms in Reciprocating Contacts. *Tribol. Int.* **2021**, *160*, 107033. [CrossRef]
24. Kandeva, M.; Stoimenov, N.; Paneva, M. Abrasive Wear of 3D Printed Polymer Materials. *J. Balk. Tribol. Assoc.* **2022**, *28*, 362–379.
25. Pawar, S.; Dolas, D. Effect of Process Parameters on Flexural Strength and Surface Roughness in Fused Deposition Modeling of PC-ABS Material. *J. Micromanuf.* **2021**, *5*, 164–170. [CrossRef]
26. Technology, I.; Ohridski, K. Investigation of abrasive wear of biodegradable. *J. Balk. Tribol. Assoc.* **2022**, *28*, 482–489.
27. Masjedi, M.; Khonsari, M.M. Grease Rheology and Film Formation. *Tribol. Int.* **2021**, *154*, 106717. [CrossRef]
28. Bazan, A.; Turek, P.; Przeszłowski, Ł. Comparison of the Contact and Focus Variation Measurement Methods in the Process of Surface Topography Evaluation of Additively Manufactured Models with Different Geometry Complexity. *Surf. Topogr. Metrol. Prop.* **2022**, *10*, 035021. [CrossRef]
29. Wang, X.; Hu, J.; Liu, J.; Liang, Y.; Wu, L.; Geng, T.; Liu, S.; Guo, Y. Tribological Performance and Enhancing Mechanism of 3D Printed PEEK Coated with In Situ ZIF-8 Nanomaterial. *Polymers* **2024**, *16*, 1150. [CrossRef]
30. Liu, S. Lubrication-Contact Boundary Conditions for Lubrication Problems. *Res. Sq.* **2021**, 1–30. [CrossRef]
31. Presilla, R.; Leckner, J.; Glavatskih, S. Grease Lubricity in the Fretting Contact: Are Ionic Liquids the Solution? *Tribol. Int.* **2023**, *185*, 108509. [CrossRef]
32. Bambu Lab. Available online: https://bambulab.com/en/x1 (accessed on 13 September 2025).
33. *ASTM G133-22*; Standard Test Method for Linearly Reciprocating Ball-on-Flat Sliding Wear. ASTM International: West Conshohocken, PA, USA, 2022.
34. *ISO 7148-2*; Plain Bearings—Testing of the Tribological Behaviour of Bearing Materials—Part 2: Testing of Polymer-Based Bearing Materials. ISO: Geneva, Switzerland, 2012.
35. *ISO 17295:2023*; Additive Manufacturing—General Principles—Part Positioning, Coordinates and Orientation. ISO: Geneva, Switzerland, 2023.
36. Hanon, M.M.; Ghaly, A.; Zsidai, L.; Klébert, S. Tribological Characteristics of Digital Light Processing (DLP) 3D Printed Graphene/Resin Composite: Influence of Graphene Presence and Process Settings. *Mater. Des.* **2022**, *218*, 110718. [CrossRef]
37. Hanon, M.M.; Zsidai, L. Comprehending the Role of Process Parameters and Filament Color on the Structure and Tribological Performance of 3D Printed PLA. *J. Mater. Res. Technol.* **2021**, *15*, 647–660. [CrossRef]

38. Stoica, C.R.; Maier, R.; Istrate, A.M.; Bucaciuc, S.G.; Despa, A. Impact Behavior Analysis of 3-D Printed Honeycomb Structures. *Mater. Plast.* **2022**, *59*, 78–90. [CrossRef]
39. Pieniak, D.; Michalczewski, R.; Firlej, M.; Krzysiak, Z.; Przystupa, K.; Kalbarczyk, M.; Osuch-Słomka, E.; Snarski-Adamski, A.; Gil, L.; Seykorova, M. Surface Layer Performance of Low-Cost 3D-Printed Sliding Components in Metal-Polymer Friction. *Prod. Eng. Arch.* **2024**, *30*, 361–376. [CrossRef]
40. Hanon, M.M.; Alshammas, Y.; Zsidai, L. Effect of Print Orientation and Bronze Existence on Tribological and Mechanical Properties of 3D-Printed Bronze/PLA Composite. *Int. J. Adv. Manuf. Technol.* **2020**, *108*, 553–570. [CrossRef]